

## Electrodeposition and Characterization of Nickel–TiN Microcomposite Coatings

Magdy A.M. Ibrahim<sup>1,2,\*</sup>, F. Kooli<sup>1</sup> and Saleh N. Alamri<sup>3</sup>

<sup>1</sup>Chemistry Department, Faculty of Science, Taibah University, Al Maddinah Al Mounwara, KSA

<sup>2</sup>Chemistry Department, Faculty of Science, Ain Shams University, 11566 Abbassia, Cairo, Egypt.

<sup>3</sup>Physics Department, Faculty of Science, Taibah University, 30002 Al Maddinah Al Mounwara, KSA

\*E-mail: [imagdy1963@hotmail.com](mailto:imagdy1963@hotmail.com)

Received: 22 April 2013 / Accepted: 28 August 2013 / Published: 25 September 2013

---

Nickel-TiN microcomposite coatings were successfully produced on copper substrate using a nickel Watts bath containing TiN microparticles via a DC electrodeposition method. The composite microstructure was characterized using fourier transform infrared spectroscopy (FTIR), X-ray diffraction (XRD) and scanning electron microscopy (SEM). The results show that the morphology of Ni-TiN microcomposite coating is sensitively dependent on the TiN microparticles concentration in the Watts bath. The corrosion behavior of the composite coatings was evaluated by anodic potentiodynamic polarization and open circuit potential measurements. The results also demonstrate that the incorporation of TiN microparticles into the nickel matrix significantly improves corrosion resistance in a 3.5% NaCl solution. Moreover, the Ni-TiN microcomposite coatings exhibit a higher hardness than a pure Ni coating.

---

**Keywords:** Composite; Nickel electrodeposition; Corrosion resistance; Titanium nitride; Microhardness; FTIR.

### 1. INTRODUCTION

Titanium nitride is a coating material that has been widely used as a thin protective film due to its high resistance to corrosion by strong acids [1], high hardness, high melting point (2927°C) and low sintering tendency, which makes it highly suited for applications in high-temperature heterogeneous catalysis [2]. TiN can be produced by physical vapour deposition (PVD) or by chemical vapour deposition at temperatures higher than 950°C. However, the major problem in using such hard coatings, in aggressive environments, is the possible presence of open porosity and pinholes in the coating, which form during the deposition process [3,4]. As a result, electrodeposition of composite coatings based on particles dispersed in a metallic matrix is gaining importance for potential

engineering applications [5]. The hard particles can be oxides, carbides, diamond, solid lubricate, nitride particles and even liquid containing microcapsules [6-14]. Electrodeposition has the advantage of easy maintenance, low working temperatures, low cost and, most importantly, the possibility of producing composite coatings with different properties, just by changing the electrodeposition operating conditions. Nowadays, TiN has become an interesting material for incorporation into a nickel matrix. In most of the previous studies, TiN particles have had an average grain size of 14-50 nm, however, in our study, the grain size are less than 10  $\mu\text{m}$ , which to the best of our knowledge is the first attempt at studying Ni-TiN composites containing micro size TiN particles.

In the present work, Ni-TiN microcomposites are prepared via a DC electrodeposition and characterized using FTIR, SEM and XRD techniques. Samples were also subjected to hardness tests as well as corrosion resistance tests in a 3.5 wt.% NaCl solution.

## 2.EXPERIMENTAL

Codeposition of Ni-TiN composite was carried out using a Watts type bath containing: 0.63 M  $\text{NiSO}_4 \cdot 6\text{H}_2\text{O}$ , 0.09 M  $\text{NiCl}_2 \cdot 6\text{H}_2\text{O}$ , 0.3 M  $\text{H}_3\text{BO}_3$  and 0.5 g/l sodium dodecyl sulfate (SDS) as an anionic surfactant and 8 g/L TiN powder at pH 3.7, 50°C and  $t = 10$  min. as optimum operating conditions. The average grain size of the TiN powder (99.7% Alfa Aesar) was less than 10  $\mu\text{m}$ . Titanium nitride particles were used as received. The extent of TiN incorporation into the nickel matrix was studied with respect to particle concentration ranging between 2 and 12  $\text{g L}^{-1}$ , and current density ranging from 0.3 to 1.6  $\text{A dm}^{-2}$ . The electroplating solutions were stirred using a magnetic stirrer for 24 h to ensure a good dispersion of TiN microparticles. The solution was then sonicated for 10 minutes before deposition. During electrodeposition, the solution was agitated with 300 rpm so as to reach the particles towards the cathode surface and improve the incorporation rate. A copper sheet (2 x 2 cm) was used as the cathode and platinum sheet as the anode. The plating cell was a rectangular Perspex trough (10 x 2.5 cm) provided with vertical grooves, on each of the side walls, to fix the electrodes. Prior to deposition, the copper cathode was pickled in a pickling solution, then washed with distilled water, rinsed with ethanol, dried and weighed. The electrodeposition was carried out galvanostatically using a DC power supply unit Model QJ3005A. At the end of the experiment, the weight of the remaining TiN in the electrolytic solution was determined by careful vacuum filtering of the TiN particles. The difference between the final and initial weight of the TiN in the solution provided the weight of TiN in the composite. The weight of the deposits gain at the cathode represents the total weight of nickel and TiN codeposited. Each experiment was repeated four times. The aqueous corrosion behavior of the composite as well as of the pure nickel was studied by using open circuit potential and anodic potentiodynamic polarization techniques.

A potentiostat/galvanostat SI 1287 Solartron, controlled by personal computer was used for the voltammetric measurements. The software packages; CorrWare 2 and CorrView 2 provided by Solartron were used to measure and analyze the data. The 3.5% NaCl solution was used as an aggressive solution for corrosion tests. A saturated calomel electrode (SCE) was used as the reference electrode and platinum sheet served as the counter electrode. To avoid crevice corrosion, protective

tape was used to mask samples, allowing  $1.0 \text{ cm}^2$  of the surface to be in contact with the solution. Anodic polarization curves were recorded between  $-600$  and  $+500 \text{ mV}$  vs SCE at a scan rate of  $5 \text{ mVs}^{-1}$ . The Ni-TiN composite coatings were investigated by Fourier transform infrared spectroscopy (Schimadzu FTIR-8400S). The crystalline structure of Ni and Ni-TiN coatings deposited on copper were examined by x-ray diffraction (Shimadzu XRD-6000) with a Ni filter and Cu  $k\alpha$  radiation. The surface morphology of the nickel and the nickel-TiN composites were examined with a Philip XL-40FEG filed emission SEM.

### 3.RESULTS AND DISCUSSION

#### 3.1. Nickel-TiN composite characterization

##### 3.1.1. FTIR measurements

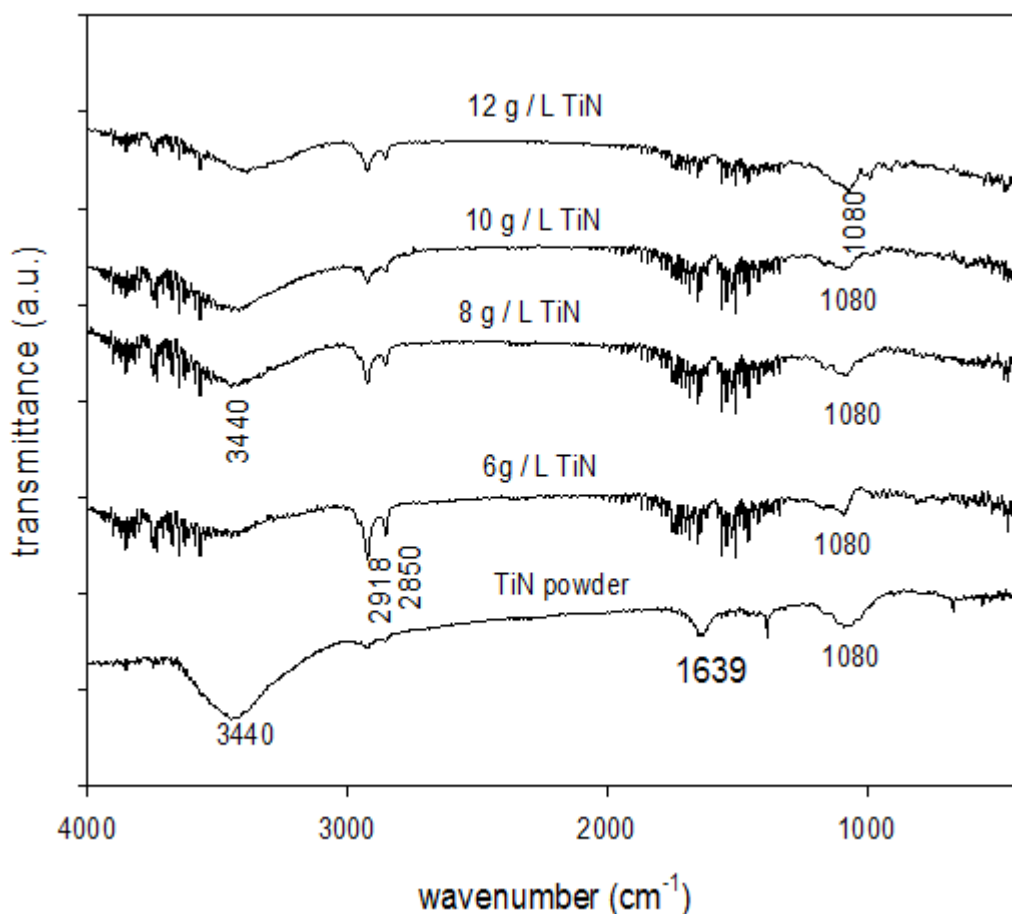
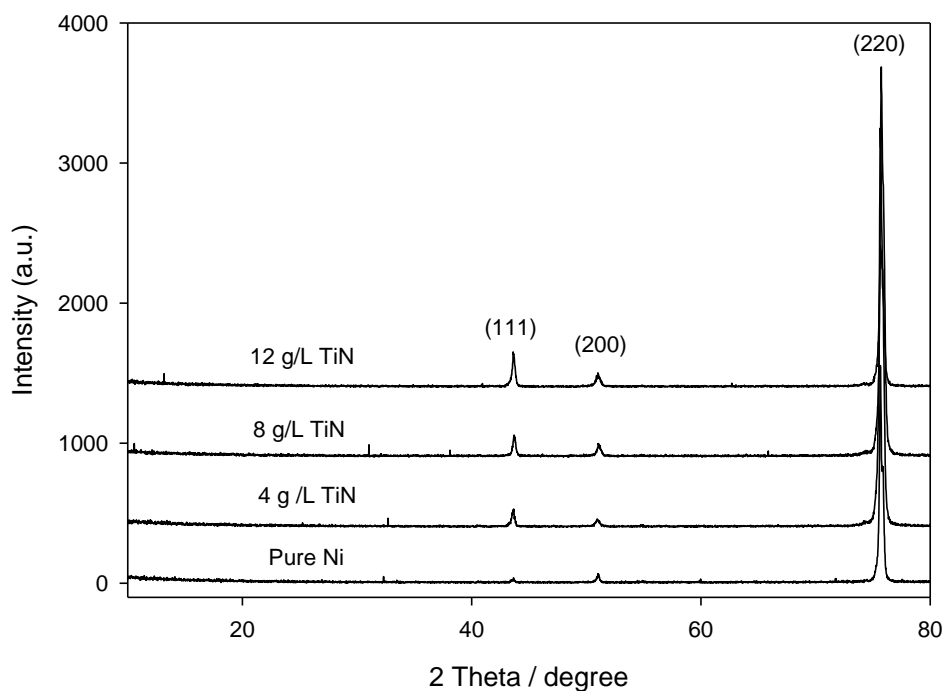


**Figure 1.** FTIR spectra of pure titanium nitride and Ni-TiN composites.

The FTIR spectra of the TiN powder and the composites are presented in Figure 1. The pure TiN powder exhibited broad bands at  $3440 \text{ cm}^{-1}$  (H-O-H stretching) and  $1639 \text{ cm}^{-1}$  (H-O-H bending), attributed to adsorbed water [15]. The presence of the band at  $1080 \text{ cm}^{-1}$ , was assigned to

TiN powder, and it was used as finger print to prove the presence of the TiN in the prepared composite. The prepared composites exhibited similar features with additional bands at 2918 and 2850  $\text{cm}^{-1}$  assigned to asymmetric and symmetric stretching bands of  $\text{CH}_2$  groups of the used surfactant [16]. The appearance of the band at 1080  $\text{cm}^{-1}$  in all of the prepared composite samples indicated clearly that the TiN particles were incorporated into the nickel matrix during the electrodeposition process.

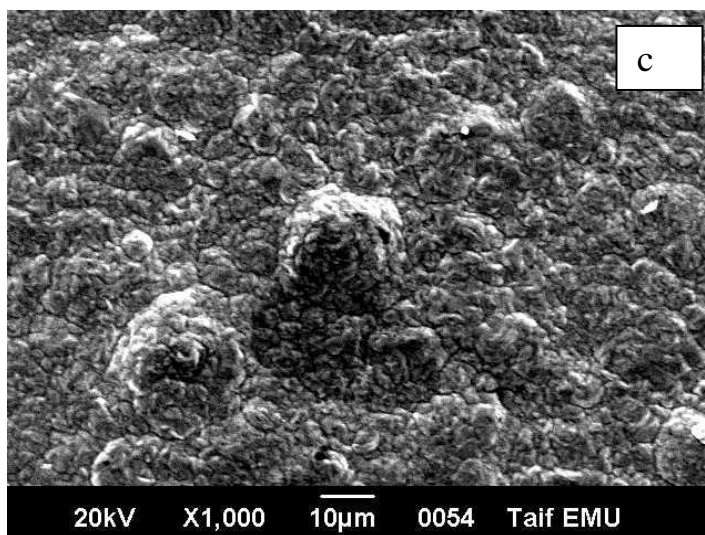
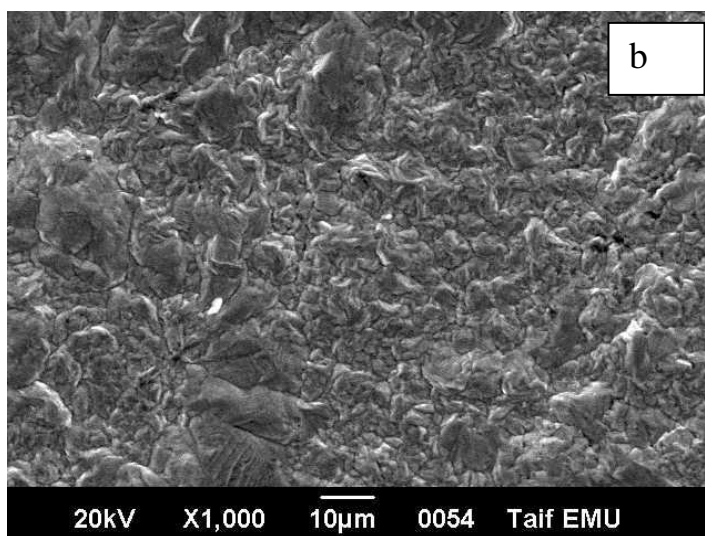
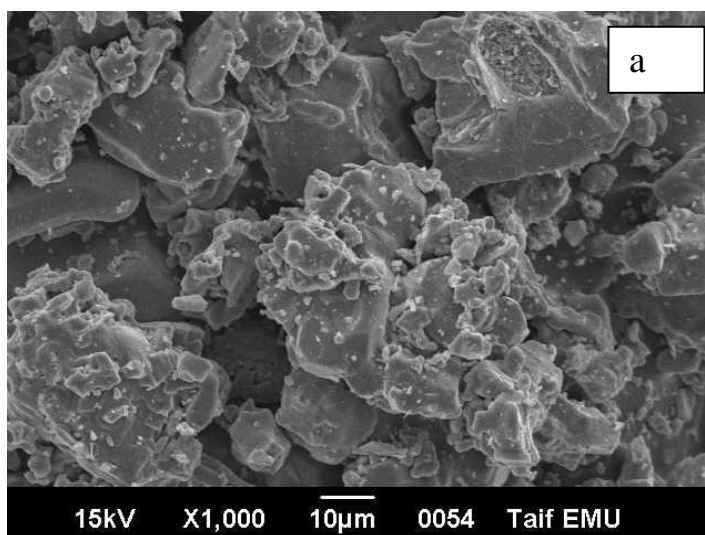
### 3.1.2. XRD analysis and surface morphology



**Figure 2.** XRD patterns for pure nickel coating and for Ni-TiN composite coatings.

The effect of TiN particles on the structure of nickel electrodeposits from Watts bath at  $\text{pH} = 3.7$ ,  $i = 1.3 \text{ Adm}^{-2}$ ,  $t = 10 \text{ min.}$  and at  $50^\circ\text{C}$  was investigated by XRD technique. The XRD patterns of pure nickel coating (Fig. 2) shows three peaks of different intensity, characteristics of a fcc structure with the highest peak intensity corresponding to the (220) preferential orientation (i.e. a highly preferred (100) growth direction). Thus, for pure nickel electrodeposition the growth mode of nickel is the normal (100) growth mode [17]. The XRD patterns of nickel coatings deposited in the presence of TiN particles reflected changes in the microstructure which were dependent on the particle content in the electrolyte. When TiN content in the electrolyte increases, i.e. TiN percentage in the coating increases, a significant increase in the intensity of peaks (111) and (200) is observed and therefore it can be conclude that the growth mode of the nickel deposit in the presence of TiN particles changes from (100) growth mode. This structural modification of nickel crystallites would be due to the incorporation of TiN particles into the nickel matrix. Similar behavior was observed by Gyawali et al

[18] and Liang et al. [19]. The effect of the incorporation of TiN particle in the nickel matrix had only negligible influence on the internal stress, which is evident from the XRD results [20].



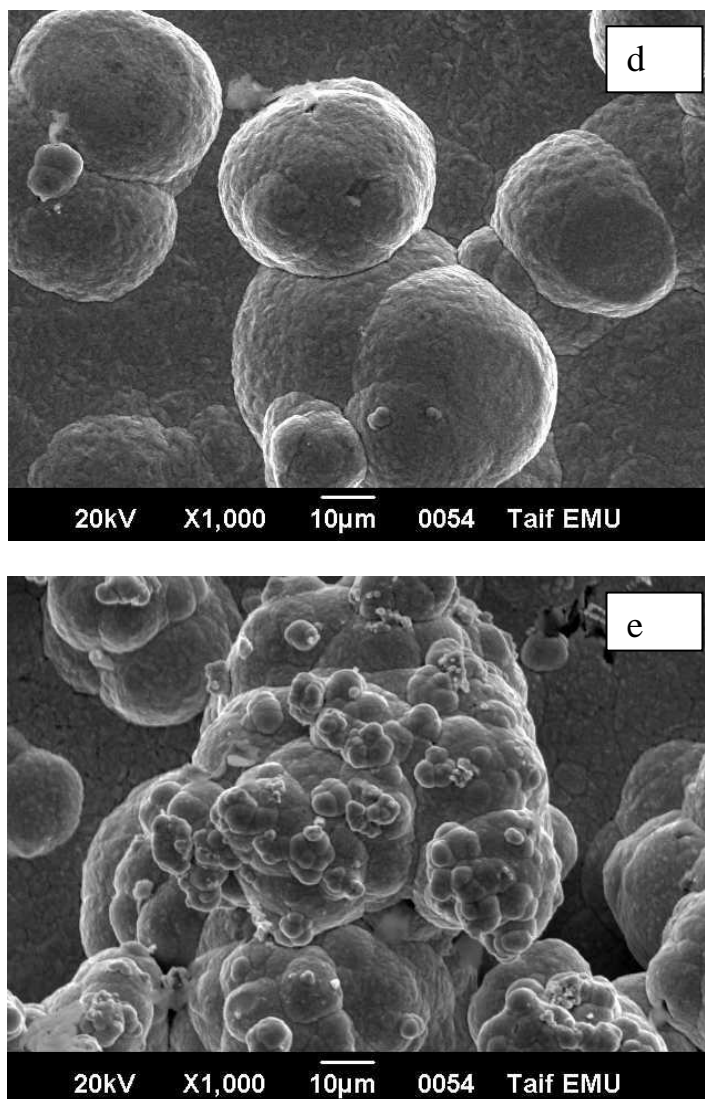


**Figure 3.** SEM photomicrographs of (a) TiN powder, (b) pure nickel coating, (c) Ni-TiN composite (2 g/L TiN), (d) Ni-TiN composite (4 g/L TiN) and (e) Ni-TiN composite (12 g/L TiN).

The photomicrograph of agglomerated TiN particles is shown in Fig. 3a. The SEM image of pure Ni deposits shows a relatively random distribution of similar nickel grains covering the entire cathode surface (Fig. 3b). On the other hand, addition of TiN particles into the plating bath leads to drastic change in morphology.

For example, addition of 2 g/L TiN starts to stimulate the agglomeration of nickel particles in the surface (Fig.3c). With further increase in TiN content in the bath (8 g/L) clusters of agglomerated particles was observed (Fig.3d). At the maximum amount of TiN added into the plating bath (12 g/L), the agglomerated particles propagated vertically on the cathode surface with big size agglomeration at the first layers ended by agglomerated particles of small size at the top (Fig.3e). The agglomeration of particles as a result of ceramic particles addition was reported by Surender et al. [21] during electrodeposition of Ni-WC composite coatings.

Therefore, it could be concluded that the addition of TiN particles to a Watts nickel plating bath and subsequent incorporation into the deposit drastically changes the surface morphology of nickel deposits and enhance the agglomeration of nickel grains of different sizes.

### 3.2. Potentiodynamic cathodic polarization curves

The potentiodynamic cathodic polarization ( $i/E$ ) curves for nickel electrodeposition on copper substrates were measured in the presence and absence of different concentrations of TiN particles in the electrolyte (Fig. 4). The curves were swept from the rest potential (about  $-0.8\text{V}$ ) up to  $-1.4\text{ V}_{\text{SCE}}$  at a scan rate of  $5\text{ mVs}^{-1}$ .

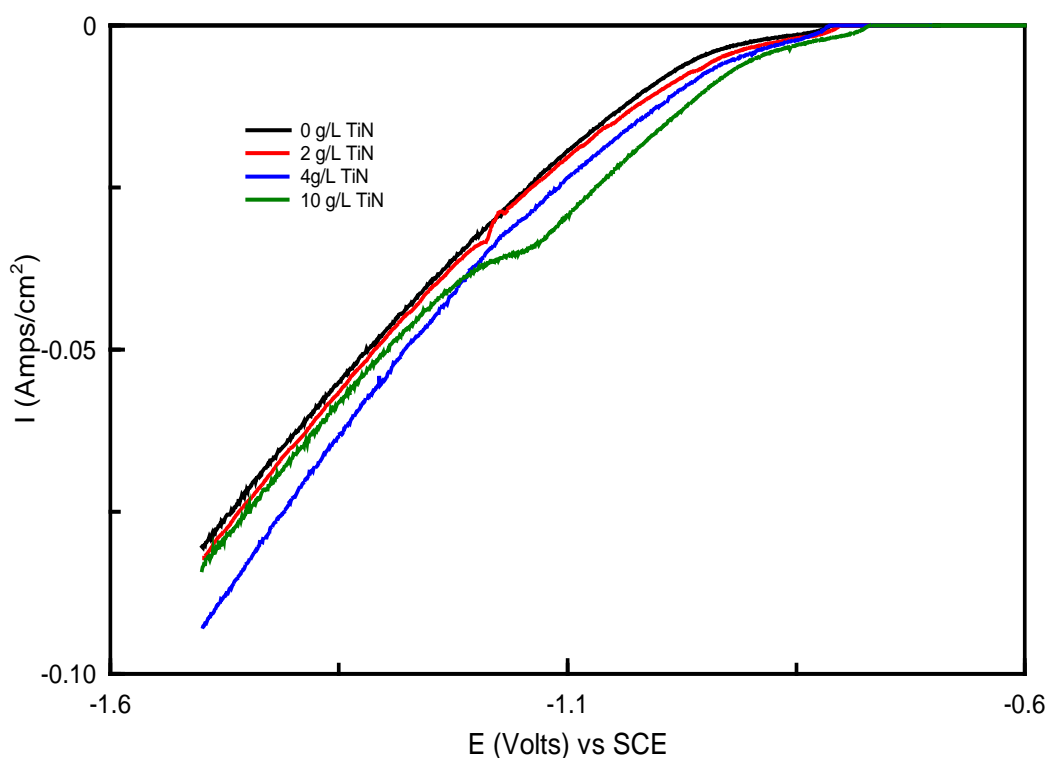


**Figure 4.** Potentiodynamic cathodic polarization curves in the presence and absence of TiN.

The addition of TiN particles has an increasing effects on the current densities of the deposition process, in addition to the marked shift in the polarization curves towards more positive potential values. This implies that TiN particles increased the rate of nickel electrodeposition, suggesting that TiN does not block the active sites on the electrode surface for nickel electrodeposition. On the contrary, it promotes nickel electrodeposition on the copper substrate. A similar observation was reported by Tulio et al. [22] during the electrodeposition of Zn in the presence of micro particles of SiC or  $\text{Al}_2\text{O}_3$ .

### 3.3. Effect of TiN particle concentration

Figure 5 shows the relationship between the weight percentage of codeposited TiN and the concentration of TiN particles in the bath (2-12 g/L) at current density of  $1.3 \text{ Adm}^{-2}$ ,  $50^\circ\text{C}$  and 300 rpm. The data shows that the amount of TiN particles in the solution has a significant effect on the weight percentage of the particles incorporated into the metal deposit. As can be seen from Fig. 5, the wt.% of TiN in the codeposited coating increases from 1.8% at 2 g/L TiN to the maximum value of 10% at 12 g/L TiN. The TiN content should correspond to the flux of TiN particles to the cathode surface multiplied by the deposition time [23]. A similar increase of ceramic content incorporated into the nickel matrix with increasing ceramic particles in the plating solutions was previously reported [24, 25].

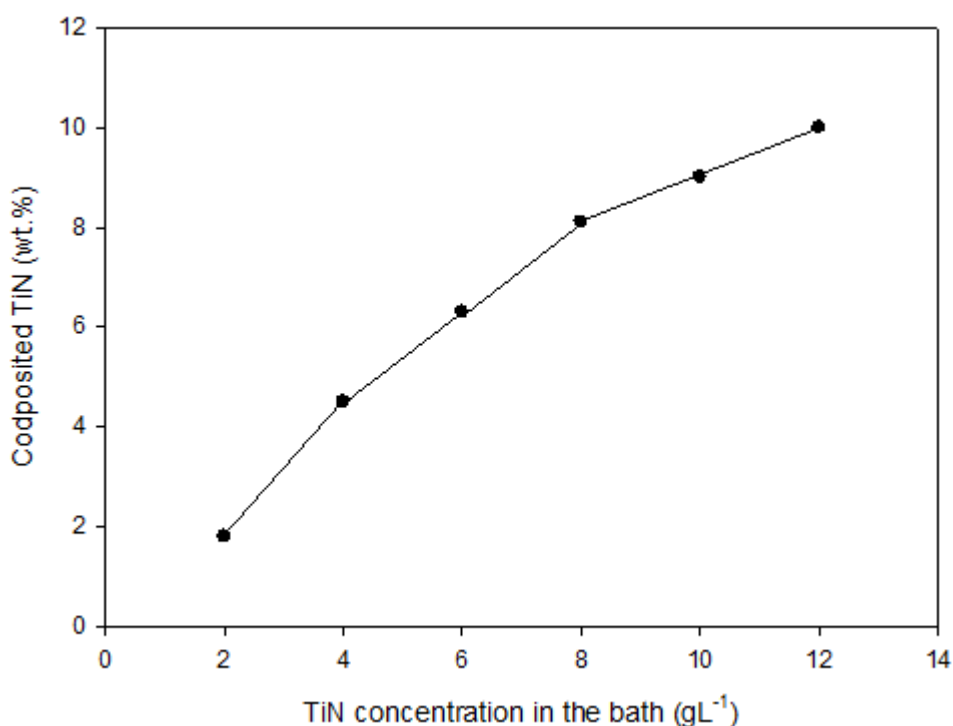


**Figure 5.** Effect of TiN concentration in the electrolyte on the TiN% in the composite. Electrodeposition conditions;  $1.3 \text{ Adm}^{-2}$ ,  $t = 10 \text{ min.}$ , pH 3.7 and  $50^\circ\text{C}$ .

### 3.4. Effect of current density

Current density variation ( $0.3 - 1.6 \text{ Adm}^{-2}$ ) had an effect on the quality of the deposits and good quality deposits were obtained between  $0.6$  and  $1.3 \text{ Adm}^{-2}$ . However, at current densities higher than  $1.6 \text{ Adm}^{-2}$  the quality of the deposits deteriorated resulting in dull and poor adherent deposits. Therefore, the effect of current density on the content of codeposited TiN particles in the coating was studied and the results are shown in Fig. 6. The TiN content in the composite increases from 1.5% at  $0.3 \text{ Adm}^{-2}$  to 10.1% at  $1.6 \text{ Adm}^{-2}$ . The amount of deposited particles is governed by the particle flux to

the metal surface [25], which is the number of particles per unit time and area deposited at a certain current density. Therefore, at the relatively lower current density range studied (0.3 – 1.6  $\text{Adm}^{-2}$ ), the particle flux increase with increase current density. A similar behavior of increasing  $\text{TiO}_2\%$  into nickel matrix with increasing current density was observed by Singh et al. [26].

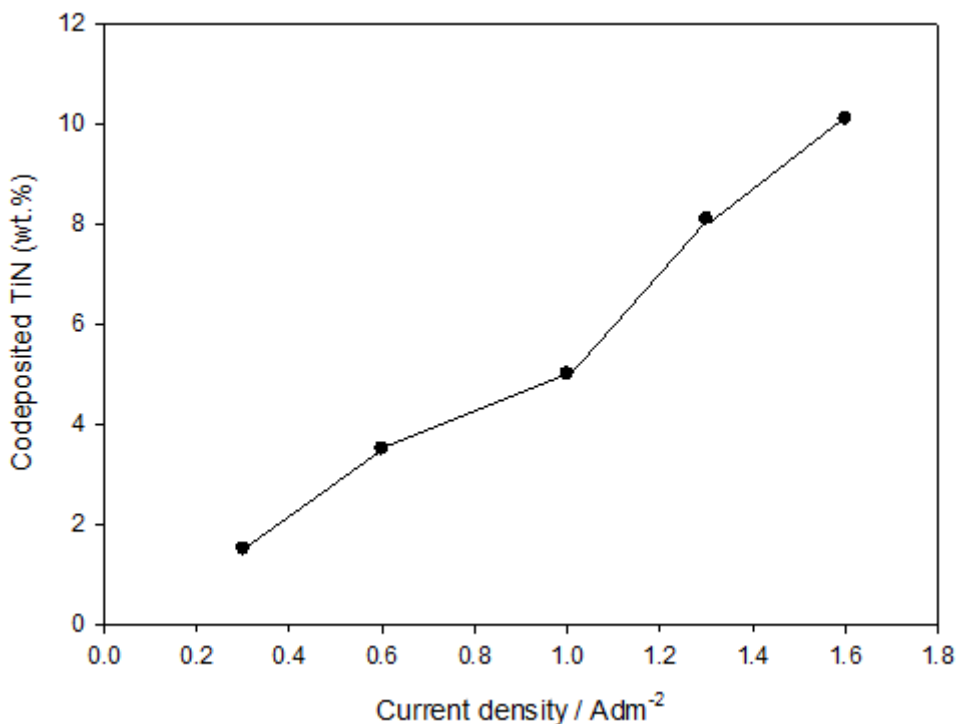


**Figure 6.** Effect of current density on the TiN% particles in the composite.

3.5. Microhardness of Ni-TiN composites

**Table 1.** Microhardness of Ni coating and Ni-TiN composite coatings

| TiN (wt.%) | Microhardness / $\text{Kg f mm}^{-2}$ |
|------------|---------------------------------------|
| 0          | 501                                   |
| 1.85       | 562                                   |
| 6.06       | 610                                   |
| 8.05       | 707                                   |
| 10.05      | 1124                                  |

Table 1 shows the microhardness of pure Ni coating and Ni-TiN micro composites obtained at  $1.3 \text{ Adm}^{-2}$ ,  $50^\circ\text{C}$ , PH 3.7,  $t = 30 \text{ min}$ . and 300 rpm. The microhardness of the composite coatings is significantly dependent on the content of TiN incorporated in the coatings. The microhardness of pure Ni coating has an average value of  $501 \text{ kg f mm}^{-2}$ . However, the microhardness of the Ni-TiN

composite coatings is higher than that of the pure Ni coating and reached to a maximum value of 1124 kg f mm<sup>-2</sup> at 12 g/L TiN. These hardness values are much higher than that reported for some other nickel composites such as Ni-carbon nanotube composite [27], nickel-CeO<sub>2</sub> composite [28], Ni-MoO<sub>3</sub> [6] and nickel-BN composite [30]. The enhancement in the hardness of Ni-TiN composite coatings is related to the dispersion-strengthening effect caused by TiN particles in the composite coatings, which impede the motion of dislocations in the metallic matrix [29]. It is very encouraging to note that the Ni-TiN composite coating exhibits higher hardness value with increasing content of the codeposited TiN particles. Accordingly, improved friction and wear properties are expected from the hardened matrix [29].

### 3.6. Electrochemical corrosion behavior

#### 3.6.1. Anodic potentiodynamic polarization

Figure 7 illustrates the potentiodynamic polarization curves of Ni-TiN composite coating and pure Ni coating deposited at the same operating conditions in 3.5wt.% NaCl solution. It could be seen in Fig. 7 that both the cathodic and anodic process of the Ni-TiN composite coating are greatly suppressed.

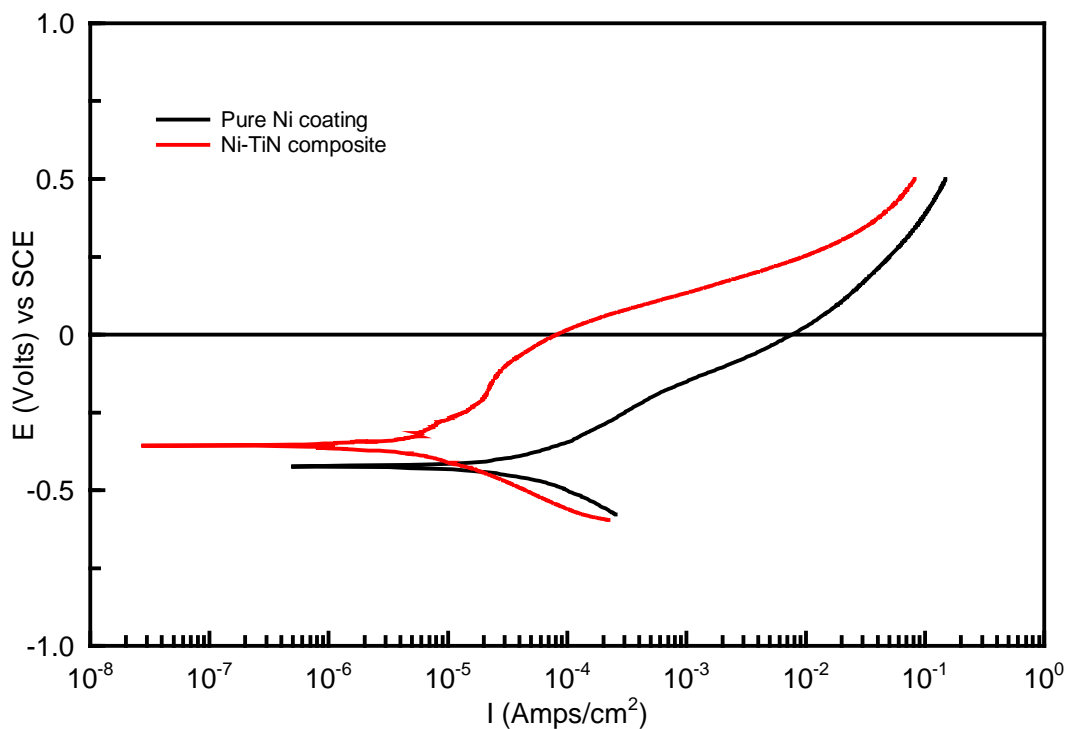


**Figure 7.** Potentiodynamic anodic polarization curves for pure nickel and Ni-TiN composite coating in 3.5% NaCl solution, with scan rate of 5 mVs<sup>-1</sup>.

This is clear from the lowering of the current density and the higher corrosion potential ( $E_{\text{corr}}$ ). The pure Ni coating shows a little active-passive transition compared to that of Ni-TiN composite

coating. The corrosion current density ( $i_{\text{corr}}$ ) and the corrosion potential ( $E_{\text{corr}}$ ) for the Ni-TiN composite coating, obtained from the polarization curves were  $8.35 \times 10^{-6} \text{ Acm}^{-2}$  and  $-0.356 \text{ V}$ , respectively; and those for the pure Ni coating were  $5.63 \times 10^{-5} \text{ Acm}^{-2}$  and  $-0.423 \text{ V}$ , respectively. Therefore, the Ni-TiN composite coating has a better corrosion resistance than the pure nickel coating. The TiN particles are inert in the potentiodynamic process, if their incorporation does not increase the number of defects, e.g. crevices between the particle and the substrate; their incorporation in the Ni coatings can reduce the effective area for the anodic dissolution, and can enhance the corrosion resistance of the coating as well.

Another possible reason for the increase in the corrosion resistance of the Ni-TiN composite might be related to the electrochemical mechanism. It has been reported previously that the dispersion of ceramic particles in the nickel matrix, which have more positive standard potential than the nickel, results in the formation of many corrosion micro cells in which the ceramics particles acts as cathode and nickel metal acts as anode [13,31]. Such corrosion micro cells facilitate the anode polarization. Therefore, in the presence of TiN particles in nickel matrix, the possibility of formation of such corrosion micro cells might be another reason for the increased corrosion resistance of the composite film.

### 3.6.2. Open circuit potential

Figure 8 shows time variations of free corrosion potential for the pure Ni and Ni-TiN composite coating in 3.5 % NaCl solution in open circuit conditions.

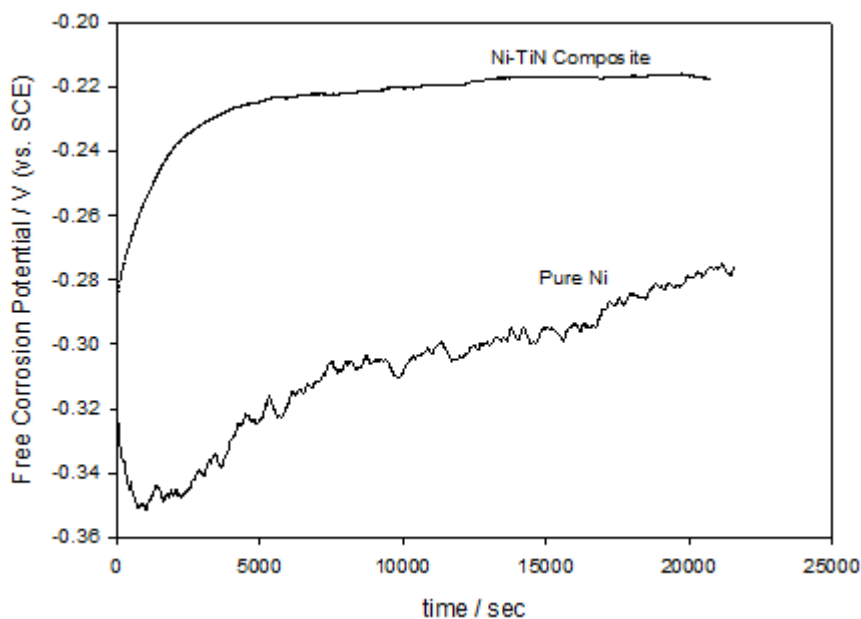


**Figure 8.** Free corrosion potential vs. time for pure Ni coating and for Ni-TiN composite coating.

The data reveal that Ni-TiN composite coating possesses nobler potentials than the pure Ni coating. Which means that Ni-TiN composite possesses a higher corrosion resistance than the pure nickel coating. This result is in good agreement with the result obtained from the anodic polarization measurements. The high value of the potential for the pure Ni coating at the beginning of immersion can be explained by the time necessary for the solution to reach the substrate by the diffusion and penetration through the nickel surface. The free corrosion potential for the composite samples reached equilibrium values (about  $-0.22 V_{SCE}$ ) within the time range of the measurements (about 6 hours). For pure nickel, the corrosion potential is shifted from  $-0.31$  to about  $-0.28 V_{SCE}$  and does not reach an equilibrium potential within the same experimental time.

It is known that an activation time, which is a period until the free corrosion potential reaches equilibrium potential, can be used for evaluation of the corrosion resistance of ceramic films coated in substrate [31,32]. This indicates continued diffusion of the solution through the surface coat to reach and attack the bare substrate. This implies that incorporation of TiN into the nickel matrix improves the corrosion resistance to a greater extent than the pure Ni alone.

#### 4. CONCLUSIONS

Analysis of the results led to the following conclusions:

- Nickel-TiN microcomposite coatings were successfully produced on copper substrate using a nickel Watts bath containing TiN microparticles via a DC electrodeposition method.
- A positive potential shift in the polarization curves is observed during the electrodeposition of nickel in the presence of TiN microparticles.
- The morphology of Ni coating is drastically changes in the presence of TiN microparticles.
- The incorporation of TiN microparticles into the nickel matrix significantly improves corrosion resistance in 3.5% NaCl solution.
- The Ni-TiN microcomposite coatings exhibited higher hardness than pure Ni coating.

#### ACKNOWLEDGMENTS

The authors gratefully acknowledge Taibahu University, KSA (grant No. 431/605).

#### References

1. H. Itoh, K. Kato and K. Sugiyama, *J. Mater. Sci.*, 21 (1986) 751.
2. S. Kaskel, K. Schlichte, G. Chaplais and M. Khanna, *J. Mater. Chem.*, 13 (2003) 1496.
3. M. A. M. Ibrahim, S.F. Korablov and M. Yoshimura, *Corros. Sci.*, 44 (2002) 81.
4. N.S. Patel, J. Menghani, K.B. Pai and M.K. Totlani, *J. Mater. Environ. Sci.*, 1(1) (2010) 34.
5. M. Ghorbani, M. Mazaheri, K. Khangholi and Y. Kharazi, *Surf. Coat. Technol.*, 148(2001)71.
6. S. Alexandridou, C.Kiparissides, J.Fransaer and J.P. Celis, *Surf. Coat. Technol.* 71 (1995) 267.
7. T.V. Sviridova, L.I. Stepanova and D.V. Sviridov, *J. Solid State Electrochem.*, 16 (2012) 3799.
8. S.T. Aruna, V. Selvi, V.K. Grips and K.S. Rajam, *J. Appl. Electrochem.*, 41 (2011) 461.
9. S. Mohajeri, A. Dolati and S. Rezagholibeiki, *Mater. Chem. Phys.*, 129 (2011) 746.

10. M.R. Vaez, S.K. Sadrnezhad and L.Nikzad, *Colloids and Surfaces Physicochem. Eng. Aspects*, 315 (2008) 176.
11. F.F. Xia, C. Liu, F. Wang, M.H. Wu, J. D. Wang, H.L. Fu and J.X. Wang, *J. Alloys and Compounds*, 490 (2010) 431.
12. C. Cai, J. Yin, Z. Zhang and J. Yang, *Mater. Sci. Forum*, 620-622 (2009) 727.
13. G.N.K.R. Bapu and S. Jayakrishnan, *Surf. Coat. Technol.*, 206 (2012) 2330.
14. F. Xia, C. Liu, C. Ma, D. Chu and L. Miao, *Int J Refract. Met. Hard Mater.*, 35 (2012) 295.
15. M. M. O. Thotiyl, T. Ravi Kumar and S. Sampath, *J. Phys. Chem. C*, 114 (2010) 1793.
16. R. P. Sperline, "Infrared spectroscopic study of the crystalline phases of sodium dodecyl sulfate," *Langmuir*, 13 (1997) 3715.
17. J. Amblard, I. Epelboin, M. Froment and G. Maurin, *J. Appl. Electrochem.*, 9 (1979) 233.
18. G. Gyawali, R. Adhikari, H.S. Kim, H.-Baek Cho and S. W. Lee, *ECS Electrochem. Lett.*, 2 (2013) C7.
19. Y. Liang, M. liu, J. Chen, X. Liu and Y. Zhou, *J. Mater. Sci. Technol.*, 27 (2011) 1016.
20. S. Ramalingam, V.S. Muralidharan and A. Subramania, *J. Solid State Electrochem.*, 13 (2009) 1777.
21. M. Surender, R. Balasubramaniam and B. Basu, *Surf.Coat. Technol.*, 187 (2004) 93.
22. P.C. Tulio and I.A. Carlos, *J. Appl. Electrochem.*, 39 (2009) 1305.
23. H.K. Lee, H.Y. Lee and J.M. Jeon, *Surf. Coat. Technol.*, 201 (2007) 4711.
24. R. Orinakova, K. Rosakova, A. Orinak, M. Kupkova, J.N. Audinot, H.-Noel Migeon, J.T. Andersson and K. Koval, *J. Solid State Electrochem.*, 15 (2011) 1159.
25. A. Sohrabi, A. Dolati, M. Ghorbani, A. Monfared and p. Stroeve, *Mat. Chem. Phys.* 121(2010) 497.
26. V.B. Singh and P. Pandey, *Surf. Coat. Technol.*, 200 (2006) 4511.
27. G. Wu, N. Li, D. Zhou, K. Mitsuo, *Surf. Coat. Technol.*, 176 (2004) 157.
28. S.-Kyu Kim and T.-Sung OH, *Trans. Nonferrous Met. Soc. China*, 21 (2011) s68.
29. Y.-Jun Xue, X.-Zhao Jia, Y.-Wei Zhou, W. Ma and J.-Shun Li, *Surf. Coat. Technol.*, 200 (2006) 5677.
30. E.Pompei, L. Magagnin, N. Lecis and P.L. Cavallotti, *Electrochim. Acta*, 54 (2009) 2571.
31. Q. Feng, T. Li, H.Teng, X.Zhang, Y.Zhang, C.Liu and J. Jin, *Surf. Coat. Technol.*, 202 (2008) 4137.
32. M. Ishikawa, K.Sugimoto, *Corros. Eng (Jpn)*, 38 (1989) 579.
33. H.E. Townsend, H.J. Clearly, L. Allegra, *Corrosion*, 37 (1981) 384.